Acta Crystallographica Section D
Biological Crystallography
ISSN 0907-4449

High-resolution neutron protein crystallography with radically small crystal volumes: application of perdeuteration to human aldose reductase

I. Hazemann,[a]‡ M. T. Dauvergne,[b] M. P. Blakeley,[b] F. Meilleur,[c] M. Haertlein,[c] A. Van Dorsselaer,[d] A. Mitschler,[a] D. A. A. Myles[b]*§ and A. Podjarny[a]*

[a]IGBMC, 1 Rue Laurent Fries, 67404 Strasbourg-Illkirch, France, [b]EMBL, 6 Rue Jules Horowitz, BP 181 Grenoble, 38042 CEDEX 9, France, [c]ILL, 6 Rue Jules Horowitz, BP 156 38042 Grenoble, France, and [d]LSMBO, CNRS UMR 7509, Universite Louis Pasteur, Faculte de Chimie, Strasbourg, France

‡ Present address: ILL, 38042 Grenoble, France.
§ Present address: Oak Ridge National Laboratory, PO Box 2008, MS6100, Oak Ridge, TN 37831, USA.

Correspondence e-mail: mylesda@ornl.gov, podjarny@igbmc.u-strasbg.fr

Received 26 May 2005
Accepted 28 July 2005

Neutron diffraction data have been collected to 2.2 Å resolution from a small (0.15 mm^3) crystal of perdeuterated human aldose reductase (h-AR; MW = 36 kDa) in order to help to determine the protonation state of the enzyme. h-AR belongs to the aldo–keto reductase family and is implicated in diabetic complications. Its ternary complexes (h-AR–co-enzyme NADPH–selected inhibitor) provide a good model to study both the enzymatic mechanism and inhibition. Here, the successful production of fully deuterated human aldose reductase [h-AR(D)], subsequent crystallization of the ternary complex h-AR(D)–NADPH–IDD594 and neutron Laue data collection at the LADI instrument at ILL using a crystal volume of just 0.15 mm^3 are reported. Neutron data were recorded to 2 Å resolution, with subsequent data analysis using data to 2.2 Å. This is the first fully deuterated enzyme of this size (36 kDa) to be solved by neutron diffraction and represents a milestone in the field, as the crystal volume is at least one order of magnitude smaller than those usually required for other high-resolution neutron structures determined to date. This illustrates the significant increase in the signal-to-noise ratio of data collected from perdeuterated crystals and demonstrates that good-quality neutron data can now be collected from more typical protein crystal volumes. Indeed, the signal-to-noise ratio is then dominated by other sources of instrument background, the nature of which is under investigation. This is important for the design of future instruments, which should take maximum advantage of the reduction in the intrinsic diffraction pattern background from fully deuterated samples.

1. Introduction

Human aldose reductase (h-AR) catalyses the NADPH-dependent conversion of glucose to sorbitol, the first step in the polyol pathway of glucose metabolism. It belongs to the aldo–keto reductase superfamily and is thought to be involved in degenerative complications of diabetes (for a recent review, see Petrash, 2004). h-AR is therefore an important target for structure-led drug design; however, despite a wealth of information from inhibitor complexes studied by X-ray crystallography, the current state of structure-based drug design has failed to proceed beyond clinical trials, owing to lack of efficacy, specificity or adverse toxic side-effect profiles. At present, only one inhibitor (epalrestat) is marketed for treatment of diabetic neuropathy (El-Kabbani, Ruiz *et al.*, 2004).

In order to improve our understanding of the interactions involved in determining the specificity and affinity of various inhibitors of h-AR, the protonation states of the active-site

residues need to be determined. X-ray electron-density maps at high resolution for h-AR complexes with different inhibitors [IDD-594, 0.66 Å (Howard *et al.*, 2004); IDD-552, 1.0 Å (Ruiz *et al.*, 2004); IDD-393, 0.9 Å (Podjarny *et al.*, 2004); fidarestat, 0.92 Å (El-Kabbani, Darmanin *et al.*, 2004)] have helped to reveal the protonation states of many residues within the active site. At these resolutions, many H atoms were visible in these complexes and the protonation states of most of the polar residues in the active site were determined. Nevertheless, even at subatomic resolution many of the labile H-atom positions were not visible, especially those with partial occupancies. The 0.66 Å X-ray structure of h-AR–NADPH–IDD594 indicates the limitations of X-ray crystallography in observation of H atoms, in particular the decreasing frequency of H-atom observation *versus* the increasing temperature factor of the bound heavy atom (Howard *et al.*, 2004). The complementarity of neutron protein crystallography and ultrahigh-resolution X-ray protein crystallography has also been described by Habash *et al.* (2000).

Neutron diffraction, on the other hand, can directly determine the positions of H atoms (and isotopes) even at moderate resolutions of ~2.0 Å. This is because the neutron scattering lengths of hydrogen, $b_n = -0.374 \times 10^{-12}$ cm, and deuterium, $b_n = +0.667 \times 10^{-12}$ cm, are closely similar to those of the common biological atoms carbon, nitrogen and oxygen (see Table 1). The enhanced visibility of H/D in neutron structures has been exploited in studies of enzyme mechanism (Kossiakoff & Spencer, 1980), in studies of ligand-binding interactions (Schoenborn, 1969; Philips & Schoenborn, 1981) and, since complete D_2O water molecules are prominent in neutron-density maps, in detailed analysis of the structure and dynamics of bound water (Cheng & Schoenborn, 1991; Daniels *et al.*, 1997; Blakeley *et al.*, 2004). Historically, however, high-resolution neutron protein crystallography has required very large crystal volumes (≥1–10 mm^3) in order to compensate for the low flux of available neutron beams. Moreover, the signal-to-noise ratio of neutron data collected from hydrogenous materials is inherently limited by the anomalously large incoherent neutron scattering cross-section of hydrogen (~80.27 barns) for thermal neutrons (*Neutron News*, 1992) which contributes to a large background under the diffracted signal. In contrast, the corresponding incoherent scattering cross section of the deuterium isotope is 2.05 barns (*Neutron News*, 1992). Isotopic substitution of deuterium for hydrogen can therefore greatly reduce the incoherent scattering background and significantly increase the signal-to-noise ratio of the data.

This can be achieved in part by H_2O/D_2O exchange of the crystal solvent prior to data collection. This approach allows H/D exchange at all solvent-accessible O- or N-atom positions in the protein, which typically accounts for 15–20% of the H-atom content of the protein. In preliminary tests, neutron Laue images collected from a partially deuterated D_2O-soaked h-AR crystal (0.15 mm^3) showed diffraction to only ~4.5 Å resolution, which is insufficient for direct determination of H-atom positions (Mitschler & Myles, unpublished results).

Table 1
Coherent scattering lengths and incoherent scattering cross-sections for atoms in biological macromolecules.

Data from *Neutron News* (1992).

	H	D	C	N	O
B_{coh} (fm)	−3.74	+6.67	+6.65	+9.36	+5.81
σ_{coh} (barns)	1.76	5.59	5.56	11.03	4.23
σ_{inc} (barns)	80.27	2.05	0	0.49	0

In order to exchange all remaining H atoms for deuterium and to further improve the signal-to-noise ratio of the data, fully deuterated protein must be produced. This can be achieved by adapting microbial expression systems for growth in fully deuterated D_2O media, which results in the expression of functional fully deuterated proteins in which all H atoms in the structure have been replaced by deuterium (Gamble *et al.*, 1994; Shu *et al.*, 2000; Tuominen *et al.*, 2004; Meilleur *et al.*, 2004). A fully deuterated system increases the Bragg scattering power and reduces the neutron scattering background (Gamble *et al.*, 1994). The corresponding gain in the signal-to-noise ratio enables neutron data to be collected in a shorter time and from smaller crystal volumes, a critical advance that makes larger unit-cell problems more accessible to study. The small crystal volume also leads to a smaller spot size, thus diminishing spot overlap at high resolution. Moreover, because the neutron scattering length of deuterium is positive and twice that of hydrogen (Table 1), D atoms are more readily visualized than H atoms in neutron-density maps, especially at moderate resolutions of ~2.0 Å (Shu *et al.*, 2000), which aids significantly in interpretation.

Here, we describe the protocol for production of fully deuterated human aldose reductase [h-AR(D)] and the subsequent crystallization of the ternary complex h-AR(D)–NADPH–IDD594 and report that good-quality neutron diffraction data extending to 2.0 Å have been collected from a small 0.15 mm^3 h-AR(D)–NADPH–IDD594 crystal on the LADI instrument at ILL. Refinement of the neutron structure of the ternary complex currently is now under way.

2. Materials and methods

2.1. Production of deuterated h-AR and purification

The deuteration protocol was adapted from those previously developed in the ILL/EMBL Deuteration Laboratory (Meilleur *et al.*, 2004, 2005). Human aldose reductase was overexpressed as a His-tagged protein using a pET 28b plasmid (Novagen) in *Escherichi coli* strain BL21 (DE3) (Novagen). Cells were adapted to fully deuterated media and grown to high cell density in a 2 l bioreactor (Infors) at 303 K using a deuterated minimal medium [6.86 g l^{-1} $(NH_4)_2SO_4$, 1.56 g l^{-1} KH_2PO_4, 6.48 g l^{-1} $Na_2HPO_4{\cdot}2H_2O$, 0.49 g l^{-1} diammonium hydrogen citrate, 0.25 g l^{-1} $MgSO_4{\cdot}7H_2O$, 1 ml l^{-1} of a trace-metal solution (0.5 g l^{-1} $CaCl_2{\cdot}2H_2O$, 16.7 g l^{-1} $FeCl_3{\cdot}6H_2O$, 0.18 g l^{-1} $ZnSO_4{\cdot}7H_2O$, 0.16 g l^{-1} $CuSO_4{\cdot}5H_2O$, 0.15 g l^{-1}

$MnSO_4{\cdot}4H_2O$, 0.18 g l^{-1} $CoCl_2{\cdot}6H_2O$, 20.1 g l^{-1} EDTA), 2 g l^{-1} deuterated succinic acid, 30 mg l^{-1} kanamycin]. Hydrated mineral salts were thoroughly dried and H atoms exchanged for deuterium by dissolution in D_2O. Cells were grown to high density in two steps, first in a batch phase and then in a fed-batch phase, where cells were continuously fed with a fresh solution of deuterated succinic acid (8%). Protein overexpression was induced with 0.5 m*M* hydrogenated IPTG at an OD_{600} of 3.0. Cells were harvested 24 h after induction, yielding ∼15 g of wet cell paste per 20 g deuterated succinic acid and 1.5 l of deuterated minimal medium. The deuterated enzyme was purified in hydrogenated (H_2O) buffers. After disruption of cells by sonication and after ultracentrifugation, the supernatant was loaded onto a Talon metal-affinity column (Clontech). Following thrombin cleavage of the His tag, the protein was loaded onto a DEAE Sephadex column (Pharmacia) and eluted against an NaCl gradient. Approximately 40 mg of deuterated h-AR(D) was recovered from 1 l culture.

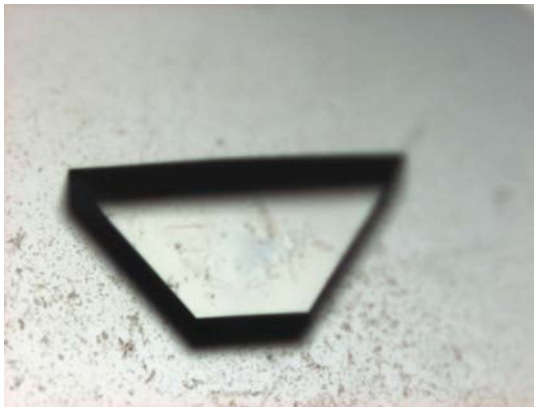

Figure 1
Fully deuterated crystal of h-AR(D) used for data collection (1.0 × 0.67 × 0.23 mm), space group $P2_1$, unit-cell parameters a = 50.11, b = 67.29, c = 47.99 Å, β = 92.5°. The twofold axis runs perpendicularly to the plate.

2.2. Co-crystallization of the deuterated enzymatic complex

As the deuterated protein was purified in H_2O, exchangeable H atoms were back-exchanged to deuterium against 50 m*M* ammonium citrate pH 5 prepared in D_2O prior to crystallization. The protein was concentrated to 30 mg ml^{-1} and mixed with the cofactor NADPH (dissolved in D_2O solution) and the inhibitor IDD-594 (dissolved in DMSO) (the protein:coenzyme:inhibitor ratio was 1:2:2). Crystallization conditions in D_2O were closely similar to those used for the hydrogenated complex (Howard *et al.*, 2004). However, we observed protein precipitation during the preparation of the hanging drops at room temperature, indicating a slight solubility decrease. Microseeding at high dilution using pre-equilibrated hanging drops (25 µl) yields crystals of average dimensions 1 × 0.6 × 0.3 mm (see Fig. 1).

2.3. Neutron data collection

A crystal of dimensions 1.0 × 0.67 × 0.23 mm (volume = 0.15 mm^3) was mounted in a quartz capillary and sealed with wax for data collection. Neutron Laue data were collected at room temperature on the LADI instrument installed on cold neutron guide H142 at ILL (Cipriani *et al.*, 1996; Myles *et al.*, 1998). The LADI instrument is equipped with a large neutron image-plate detector mounted on a cylindrical camera, which completely encircles the sample. An Ni/Ti multi-layer band-pass filter was used to select a restricted wavelength range ($\delta\lambda/\lambda$ = 25%) centred at 3.3 Å and extending from 2.9 to 3.7 Å. Data were recorded in a series of contiguous Laue images with a step separation of Φ = 7° around the horizontal rotation axis of the camera. Two data sets were collected from the same crystal: the first 30 frames with the capillary mounted along the rotation axis and then 32 frames with the crystal in a second orientation (45° away from the rotation axis). The exposure time for each frame was typically 36 h.

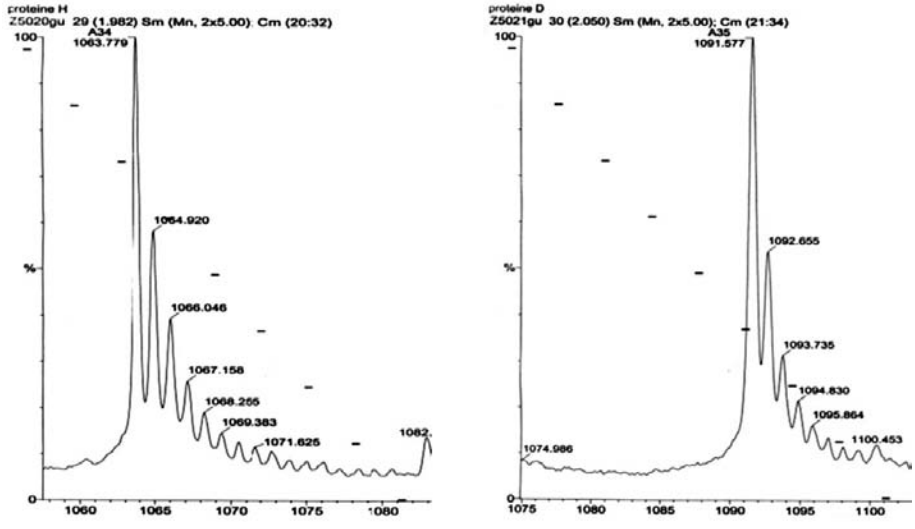

Figure 2
Electrospray mass spectrometry (m/z plot) of hydrogenated protein (left) and deuterated protein (right). The molecular-weight increase of 6% from h-AR(H) [MW = 36 134.6 (2) Da] to h-AR(D) [MW = 38 169.6 (2) Da] indicates full deuteration of the protein.

Spots were observed to 2.0 Å resolution, a clear improvement from the ∼4.5 Å resolution observed from the partially deuterated D_2O-soaked h-AR crystal (0.15 mm^3). A qualitative comparison of the diffraction patterns from the fully and partially deuterated similar crystals showed an increase in the height of the Bragg spots of ∼2.5–3-fold. Theoretical calculations show an increase of coherent scattering power from the non-exchangeable D atoms of 2.5, which is in good agreement with the experimental value. With regard to the background, we observe an overall decrease of a factor of ∼2.

Since the incoherent scattering from the crystal is theoretically diminished around 16 times in the fully deuterated case, we have to assume that a strong noise is arising from other sources. The reduction in background with perdeuteration was a factor of 8 less than expected, presumably because of the now dominant contribution of other possible sources of instrument background (*e.g.* γ-rays accumulated during long exposure times). The nature and origin of this background component is under investigation at the LADI instrument. This is important for the design of future instruments, which should take maximum advantage of the reduction in the intrinsic diffraction pattern background from fully deuterated samples.

3. Results

3.1. Determination of deuteration level

The deuteration level of the protein was checked by electrospray mass spectrometry (*m*/*z* plot; Van Dorsselaer, private communication). The spectra for both hydrogenated protein (left) and deuterated protein (right) are shown in Fig. 2. The molecular-weight difference of 38 169.6 (2) Da for h-AR(D) compared with 36 134.4 (2) Da for h-AR(H) indicates a deuteration level close to 100%.

3.2. X-ray data collection and processing

The quality of fully deuterated crystals grown in the same batch as the crystal used for neutron data collection has been verified by X-ray data collection at SBC-APS [Joachimiak *et al.*, private communication; T = 15 K (helium cooling), $d_{\min}$ = 0.8 Å, $R_{\rm merge}$ = 2.3%, refined average mosaicity = 0.22°) and at the Swiss Light Source (SLS) (Schulze Briese *et al.*, private communication; T = 293 K, $d_{\min}$ = 1.8 Å, $R_{\rm merge}$ = 5%, refined average mosaicity = 0.05°).

3.3. Neutron data collection and processing

Neutron Laue data were processed using the Daresbury Laboratory *LAUEGEN* software suite (Helliwell *et al.*, 1989; Campbell, 1995), modified for the cylindrical geometry of the LADI detector (Campbell *et al.*, 1998). The *LAUEGEN* program was used to index (space group $P2_1$) and refine the orientation for each of the crystal settings, to refine the unit-cell parameters at room temperature (a = 50.11, b = 67.29, c = 47.99 Å, β = 92.50°) and to predict and integrate the reflections on each frame. The *LSCALE* program (Arzt *et al.*, 1999) was used to derive the wavelength-normalization curve (Fig. 3) using the intensities of symmetry-equivalent reflections measured at different wavelengths within the wavelength range 2.9–3.7 Å. Data recorded at λ < 2.9 Å were in poor agreement with the remainder of the data, most likely as a consequence of the fall-off in spectral intensity distribution and thus were excluded. No account was made for crystal damage since neutrons do not induce detectable radiation damage and no explicit absorption corrections were applied.

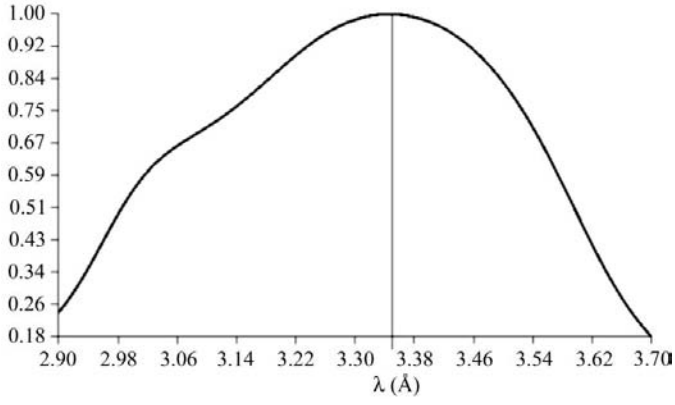

Figure 3
Neutron Laue wavelength-normalization curve.

Table 2
Summary of 2.2 Å neutron Laue diffraction data from fully deuterated h-AR complex.

$d_{\min}$ (Å)	No. of observations	No. of reflections	Completeness (%)	$I/\sigma(I)$	$R_{\rm merge}(I)$	Multiplicity
6.96	1958	487	91.6	7.6	0.124	4.0
4.92	5370	887	92.9	8.9	0.170	6.1
4.02	7806	1152	94.6	9.1	0.204	6.8
3.48	6418	1296	89.7	6.7	0.233	5.0
3.11	5259	1362	83.6	5.1	0.254	3.9
2.84	4367	1338	75.1	4.2	0.249	3.3
2.63	3891	1327	68.5	3.7	0.262	2.9
2.46	3778	1353	64.3	3.4	0.262	2.8
2.32	3810	1329	60.5	3.3	0.272	2.9
2.20	3662	1354	57.6	2.9	0.271	2.7
Overall	46319	11885	73.5	5.1	0.228	3.9

Finally, *SCALA* (Collaborative Computational Project, Number 4, 1994) was used to combine and merge the observed reflections to produce a final data set of 11 885 unique reflections to 2.2 Å resolution with an overall merging R factor of 22.8% (12.4% at low to 27.1% at high resolution) and $\langle I/\sigma(I)\rangle$ = 5.1 (2.9 in the outer shell) with completeness 73.5% (57.6% in the outer shell) and multiplicity 3.9 (2.7 in the outer shell) (see Table 2).

This data set is currently being used for the refinement of the h-AR(D)–NADP$^+$–IDD594 complex. The signal of the D atoms appears clearly, as shown in Fig. 4. The fully refined structure and its implications for the catalytic mechanism will be published later.

4. Conclusion and outlook

This work represents the first reported example of a successful neutron protein crystallography analysis of such a large (36 kDa) fully deuterated protein using a small sub-millimetre crystal of just 0.15 mm^3. This is a significant milestone in neutron protein crystallography research, which until now has required very large sample volumes of >>1–10 mm^3. The key to this success was the ability to produce fully deuterated human aldose reductase crystals, which improved the Bragg scattering by a factor of 2.5 and reduced the large hydrogen incoherent scattering leading to a background reduction of roughly 50%, thus enhancing the signal-to-noise ratio of the neutron data in a major way. We believe that the demon-

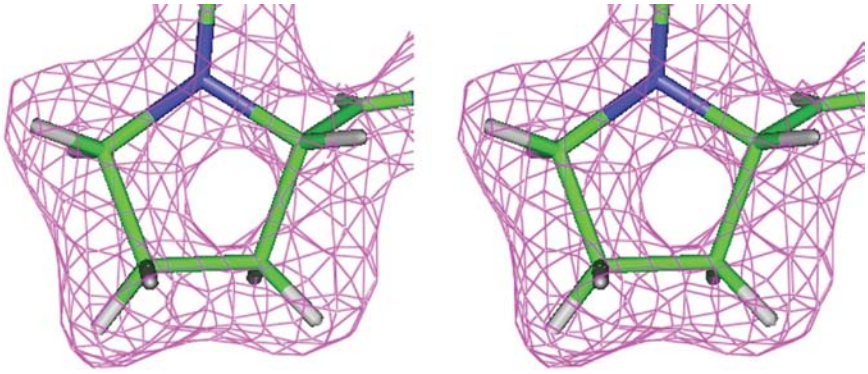

Figure 4
Neutron scattering density map ($2F_o - F_c$, 1.5 r.m.s. contours) superposed with the current model of aldose reductase for Pro13. Note the clear density for the D atoms.

stration of this capability will have a major impact on the field of neutron protein crystallography and that deuterium labelling will make possible experiments on smaller crystals of larger proteins systems that would otherwise have been intractable.

This work also represents a significant advance in our work on human aldose reductase. Refinement of the neutron structure is under way and shows enhanced visibility for all protons (as deuterons) in the ternary complex. The direct determination of the protonation states of the residues within the active site is crucial for a more complete understanding of the enzymatic mechanism and thus the inhibition. More specifically, the protonation state of His110 and the orientation of the hydroxyl group of Tyr48 are of particular interest. The supplementary information derived from the neutron data may be used in a more rational approach to drug design and for the design of new novel inhibitors.

We thank the staff of the Department of Structural Biology and Genomics of the IGBMC for their support, the synchrotron staff of SBC-APS USA and SLS Switzerland for their help, the ILL Scientific Committee for their support of this long-term project, F. Dauvergne for skilled technical support on LADI at ILL and the Institute for Diabetes Discovery for providing the inhibitor IDD594. This work was supported by the Centre National de la Recherche Scientifique (CNRS), by the Institut National de la Sante et de la Recherche Medicale (INSERM) and by the Hôpital Universitaire de Strasbourg (HUS). DAAM acknowledges the support of the Laboratory Directed Research and Development Program of Oak Ridge National Laboratory, DOE Contract No. DE-AC05-00OR22725.

References

Arzt, S., Campbell, J. W., Harding, M. M., Hao, Q. & Helliwell, J. R. (1999). *J. Appl. Cryst.* **32**, 554–562.
Blakeley, M. P., Kalb (Gilboa), A. J., Helliwell, J. R. & Myles, D. A. A. (2004). *Proc. Natl Acad. Sci. USA*, **101**, 16405–16410.
Campbell, J. W. (1995). *J. Appl. Cryst.* **28**, 228–236.
Campbell, J. W., Hao, Q., Harding, M. M., Nguri, N. D. & Wilkinson, C. (1998). *J. Appl. Cryst.* **31**, 496–502.
Cheng, X. D. & Schoenborn, B. P. (1991). *Acta Cryst.* A**47**, 314–317.
Cipriani, F., Castagna, J. C., Wilkinson, C., Oleinek, P. & Lehmann, M. S. (1996). *J. Neutron Res.* **4**, 79–85.
Collaborative Computational Project, Number 4 (1994). *Acta Cryst.* D**50**, 760–763.
Daniels, B. V., Schoenborn, B. P. & Korszun, Z. R. (1997). *Acta Cryst.* D**53**, 544–550.
El-Kabbani, O., Darmanin, C., Schneider, T. R., Hazemann, I., Ruiz, F., Oka, M., Joachimiak, A., Schulze-Briese, C., Tomizaki, T., Mitschler, A. & Podjarny, A. (2004). *Proteins*, **55**, 805–813.
El-Kabbani, O., Ruiz, F., Darmanin, C. & Chung, R. P.-T. (2004). *Cell. Mol. Life Sci.* **61**, 750–762.
Gamble, T. R., Clauser, K. R. & Kossiakoff, A. A. (1994). *Biophys. Chem.* **53**, 15–25.
Howard, E., Sanishvili, R., Cachau, R. E., Mitschler, A., Chevrier, B., Barth, P., Lamour, V., Van Zandt, M., Sibbley, E., Bon, C., Moras, D., Schneider, T. R., Joachimiak, A. & Podjarny, A. (2004). *Proteins*, **55**, 792–804.
Habash, J., Raftery J., Nuttall, R., Price, H. J., Wilkinson, C., Kalb (Gilboa), A. J. & Helliwell, J. R. (2000). *Acta Cryst.* D**56**, 541–550.
Helliwell, J. R., Habash, J., Cruickshank, D. W. J., Harding, M. M., Greenhough, T. J., Campbell, J. W., Clifton, I. J., Elder, M., Machin, P. A., Papiz., M. Z. & Zurek, S. (1989). *J. Appl. Cryst.* **22**, 483–497.
Kossiakoff, A. A. & Spencer, S. A. (1980). *Nature (London)*, **288**, 414–416.
Meilleur, F., Contzen, J., Myles, D. A. A. & Jung, C. (2004). *Biochemistry*, **43**, 8744–8753.
Meilleur, F., Dauvergne, M.-T., Schlichting, I. & Myles, D. A. A. (2005). *Acta Cryst.* D**61**, 539–544.
Myles, D. A. A., Bon, C., Langan, P., Cipriani, F., Castagna, J. C., Lehmann, M. S. & Wilkinson, C. (1998). *Phys. B*, **241**, 1122–1130.
Neutron News (1992). Vol. 3, No. 3, pp. 29–37.
Petrash, J. M. (2004). *Cell. Mol. Life Sci.* **61**, 737–749.
Philips, S. E. & Schoenborn, B. P. (1981). *Nature (London)*, **291**, 81–82.
Podjarny, A., Cachau, R. E., Schneider, T., Van Zandt, M. & Joachimiak, A. (2004). *Cell. Mol. Life Sci.* **61**, 763–773.
Ruiz, F., Hazemann, I., Mitschler, A., Joachimiak, A., Schneider, T., Karplus, M. & Podjarny, A. (2004). *Acta Cryst.* D**60**, 1347–1354.
Schoenborn, B. P. (1969). *Nature (London)*, **224**, 143–146.
Shu, F., Ramakrishnan, V. & Schoenborn, B. P. (2000). *Proc. Natl Acad. Sci. USA*, **97**, 3872–3877.
Tuominen, V. U., Myles, D. A. A., Dauvergne, M. T., Lahti, R., Heikinheimo, P. & Goldman, A. (2004). *Acta Cryst.* D**60**, 606–609.